10

Summary on Uniaxial Ratchetting of 6061-T6 Aluminium Alloy

Guozheng Kang, Jun Ding and Yujie Liu
Department of Applied Mechanics and Engineering, Southwest Jiaotong University
China

1. Introduction

Aluminium alloys are currently being used as major structure components in automobiles, high-speed railway vehicles and aircrafts, which are often subjected to a cyclic loading. It is necessary to predict their cyclic responses as accurately as possible by constructing new constitutive models before the strength, fatigue life and safety of structure components can be assessed reasonably. During asymmetrical stress-controlled cyclic loading, a cyclic accumulation of inelastic deformation, i.e., ratchetting will occur in the materials. The ratchetting is an important factor which should be carefully considered in the assessment of fatigue failure and safety of structures, and has been extensively studied for three decades by many researchers as reviewed by Ohno (1990; 1997), Bari and Hassan (2002), Kang (2008), and Chaboche (2008). The existing work shows that the cyclic softening/hardening feature of materials, and the loading level, history, path, rate, and waveform, as well as ambient temperature have great effect on the ratchetting behaviour of materials. Based on the experimental observations, some phenomenological cyclic elasto-plastic and viscoplastic constitutive models have been constructed to describe the uniaxial and multiaxial ratchetting of metal materials. The established models are mainly obtained by extending the nonlinear kinematic hardening rules originally developed by Armstrong and Frederick (1966) and revised by Chaboche (1991), Ohno and Wang (1993a; 1993b), Jiang and Sehitoglu (1996), Abdel-Karim and Ohno (2000), Kang et al (2003), Chen and Jiao (2004), Kan et al (2007), and Kang et al (2009) and so on. However, most of the researches concerned the ratchetting behaviours of stainless steels and other carbon steels. A few papers addressed the ratchetting behaviours of aluminium and its alloys, e.g., the papers published by Chen and Abel (1996), Yang et al (1998), Hu et al (1999), and Ding et al (2008) for 2014-T6, pure aluminium, 7050-T7451, and LY12-CZ aluminium alloys, respectively. Such results show that the ratchetting behaviours of aluminium alloys also differ greatly from different types of the alloys. Recently, the authors have also accomplished some experimental and theoretical researches for the uniaxial time-dependent ratchetting behaviour of 6061-T6 alloy at room and high temperatures, and its ratchetting-fatigue interaction (Ding et al, 2007; Kang et al, 2008; Ding et al, 2010) and obtained some significant conclusions which are very useful to realize the ratchetting behaviours of aluminium alloys and predict them accurately in the future work.

Therefore, in this Chapter, some experimental and theoretical results about the uniaxial ratchetting and ratchetting-fatigue interaction of 6061-T6 aluminium alloy are provided to

demonstrate our attempt to launch more comprehensive research about the ratchetting behaviour of aluminium alloys in the future. Based on the detailed tests, the dependences of uniaxial ratchetting of the alloy on the stress level, stress rate, peak stress hold and ambient temperature are investigated, and then a new cyclic constitutive model is proposed to describe the ratchetting of aluminium alloy reasonably. In the proposed model, a new kinematic hardening rule is employed to represent the time-dependence of ratchetting behaviour of aluminium alloy at room and high temperatures.

2. Experimental procedure

As-received 6061-T6 aluminium alloy is used as the experimental material in our researches, as discussed in Ding et al (2007), Kang et al (2008), and Ding et al (2010). The chemical composition of the alloy in mass percentage is: Cu, 0.15-0.40%; Si, 0.4-0.8%; Fe, 0.7%; Mn, 0.15%; Mg, 0.8-1.2%; Zn, 0.25%; Cr, 0.04-0.35%; Ti, 0.15%; Al, remained. Cylindrical specimens are manufactured directly from the as-received 6061-T6 bars. The specimens for the tests at room temperature have gauge length of 10 mm and cross-section diameter of 6 mm; while those for the tests at high temperature have gauge length of 30 mm and cross-section diameter of 6 mm. All the tests are performed in MTS-809-25kN machine with a temperature controlling system of MTS653. The experimental procedure and data are controlled and collected by TestStar system attached to the test machine, respectively. The specimens are investigated under the uniaxial strain- and stress-controlled cyclic loading tests (simplified as uniaxial cyclic straining and stressing, respectively) at the strain rate of $2\times10^{-3}\cdot s^{-1}$ and stress rate of 100 $MPa\cdot s^{-1}$, respectively, except for the cases specified. The tests are performed at room temperature and 150˚C. In some cases, the specimens are tested till the fracture occurs, in order to investigate the ratchetting-fatigue interaction of the alloy. To demonstrate the ratchetting behaviour of 6061-T6 aluminium alloy more clearly, the curves of ratchetting strain vs number of cycles are illustrated in the figures in the next section, based on the following definition of uniaxial ratchetting strain ε_r:

$$\varepsilon_r=(\varepsilon_{max}+\varepsilon_{min})/2 \quad (1)$$

Where ε_{max} and ε_{min} are the maximum and minimum axial strains measured after each cycle, respectively.

3. Experimental results

3.1 Uniaxial time-dependent ratchetting behaviour

At first, 6061-T6 aluminium alloy is tested under monotonic tension and uniaxial strain-controlled cyclic loading to realize some basic performances of the alloy and determine the loading conditions for the uniaxial ratchetting tests discussed in the next section. Fig. 1 shows the results of monotonic tension obtained at different strain rates and at room temperature and 150˚C. It is seen from Fig. 1 that the alloy presents apparent rate-dependent deformation during the monotonic tension, and the tensile stress-strain curve of the alloy is higher at faster strain rate. However, the degrees of rate-dependence for the alloy at room temperature and 150˚C are almost the same, which can be concluded by comparing the results shown in Fig. 1a and Fig. 1b.

Fig. 2 gives the results of responded stress amplitude evolving with increasing number of cycles under the uniaxial cyclic straining with applied strain amplitude of 0.6% and with or

without peak/valley strain hold. And Fig. 3 shows the results in the cyclic straining with only peak strain hold and at 150˚C, where the applied strain amplitude is also 0.6%.

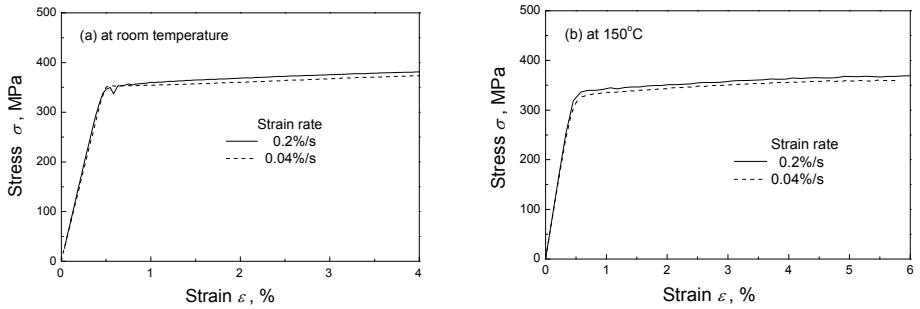

Fig. 1. Tensile stress-strain curves of the alloy at different strain rates: (a) at room temperature; (b) at 150˚C. (Originally from Ding et al. (2007))

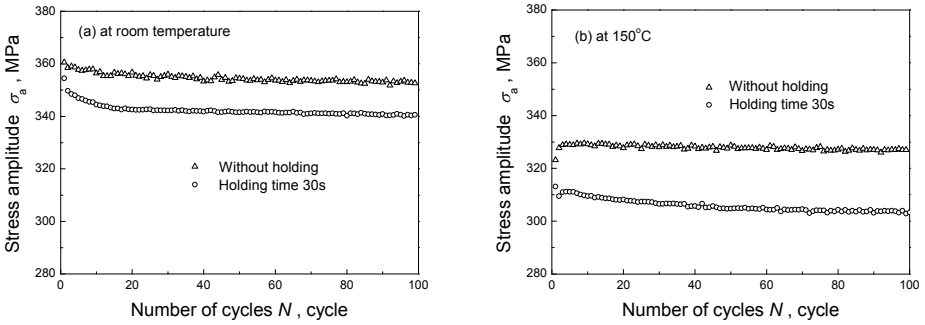

Fig. 2. Curves of responded stress amplitude vs number of cycles for the alloy during the cyclic straining with or without peak/valley strain hold: (a) at room temperature; (b) at 150˚C. (Originally from Ding et al. (2007))

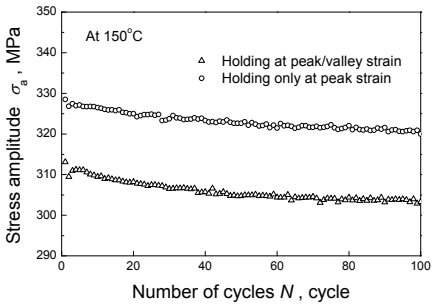

Fig. 3. Curves of responded stress amplitude vs number of cycles for the alloy during the cyclic straining with only peak strain hold and at 150˚C. (Originally from Ding et al. (2007))

It is shown that the as-received 6061-T6 aluminium alloy presents apparent cyclic softening feature at room temperature and 150˚C, and the responded stress amplitude continuously decreases with the increasing number of cycles. Also, the cyclic softening behaviour of the alloy is time-dependent, and the curves of responded stress amplitude vs number of cycles without any peak/valley strain hold are higher than those with certain peak/valley strain hold, as shown in Fig. 2a and 2b. Moreover, the responded stress amplitude of the alloy during the cyclic straining with only peak strain hold is also higher than that with peak/valley strain hold, as shown in Fig. 3. The decreased responded stress amplitude during the cyclic straining with peak/valley strain hold is caused by the stress relaxation occurred in the peak and/or valley strain hold due to the viscosity of the alloy. It should be noted from Fig. 2 that during the strain-controlled cyclic loading, the time-dependent cyclic softening feature of the alloy is more remarkable at 150˚C than that at room temperature, which is different from the rate-dependent feature presented in the monotonic tensions with different strain rates. It implies that the viscosity of the alloy is more remarkable at 150˚C than at room temperature.

Then the alloy is tested under the uniaxial asymmetrical stress-controlled cyclic loading with different applied stresses and at constant stress rate. The uniaxial ratchetting of 6061-T6 aluminium alloy and its dependence on the applied stress level and loading history are observed at room temperature and 150˚C. The results are shown in Fig. 4 to Fig. 6.

It is concluded from the figures that: (1) Ratchetting occurs progressively in the alloy during the asymmetrical uniaxial cyclic stressing at room temperature and 150˚C. The ratchetting strain increases with the increasing number of cycles, but the ratchetting strain rate (e.g., the increment of ratchetting strain after each cycle) decreases gradually during the cyclic stressing, as shown Fig. 4 and Fig. 5. It should be noted that the exception illustrated in Fig. 5 and occurred in the loading case of 30±300MPa (i.e., the applied mean stress is 30 MPa, and stress amplitude is 300 MPa), i.e., the increasing ratchetting strain rate after 60 cycles is mainly caused by the fluctuation of temperature during the test at 150˚C. (2) The ratchetting of the alloy depends on the applied stress level, and the ratchetting strain increases with the increasing mean stress and stress amplitude. The evolution of ratchetting behaviour of the alloy at room temperature is similar to that at 150˚C, as shown Fig. 4 and Fig. 5. (3) The ratchetting of the alloy also depends on the loading history, and the previous cyclic stressing with higher stress level can restrain the occurrence of ratchetting in the alloy in the sequent cyclic stressing with lower stress level, as shown in Fig. 6 for the multi-stepped cyclic loading of 20±340MPa (200c) → 30±340MPa (200c) → 20±340MPa (100c). (4) After certain cycles, a stable evolution of ratchetting with a constant ratchetting strain rate is reached due to the cyclic softening feature of 6061-T6 aluminium alloy and no shakedown of ratchetting occurs. This is different from that of stainless steels commented by Kang (2008), where a quasi-shakedown of ratchetting occurs due to the cyclic hardening feature of stainless steels.

Finally, the alloy is tested under the uniaxial asymmetrical stress-controlled cyclic loading at different stress rates and with or without peak stress hold, respectively. The uniaxial time-dependent ratchetting of 6061-T6 aluminium alloy is observed at room temperature (loading case of 30±340MPa) and 150˚C (loading case of 30±300MPa). The results are shown in Fig. 7 and Fig. 8. It is concluded from the figures that the ratchetting of the alloy presents apparent time-dependence. The values of ratchetting strain produced during the cyclic stressing at lower stress rate and with certain peak stress hold are much larger than those at higher stress rate and without peak stress hold, respectively, both at room temperature and 150˚C. Furthermore, the ratchetting strain increases remarkably with the increasing hold time at peak stress point.

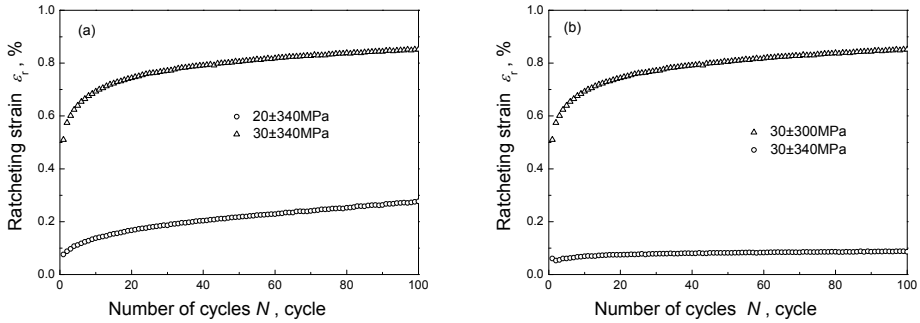

Fig. 4. Ratchetting of the alloy at room temperature: (a) with various mean stresses; (b) with various stress amplitudes. (Originally from Ding et al. (2007))

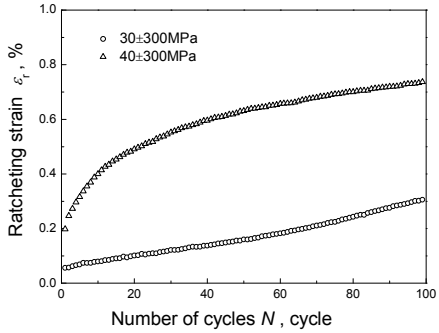

Fig. 5. Ratchetting of the alloy with various mean stresses and at 150˚C. (Originally from Ding et al. (2007))

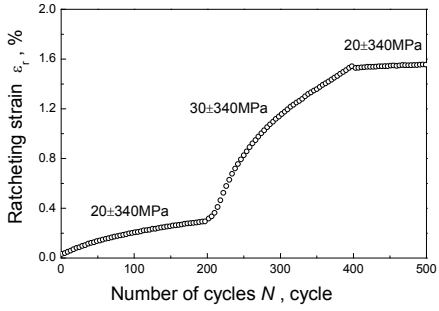

Fig. 6. Ratchetting of the alloy with multi-stepped stress levels at room temperature. (Originally from Ding et al. (2007))

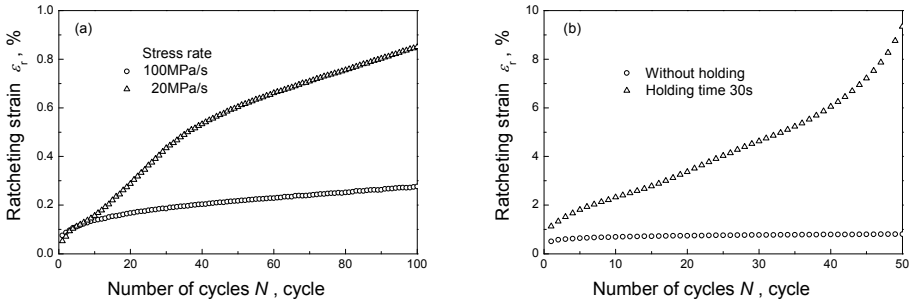

Fig. 7. Time-dependent ratchetting of the alloy at room temperature (30±340MPa): (a) at two stress rates; (b) with or without peak stress hold. (Originally from Ding et al. (2007))

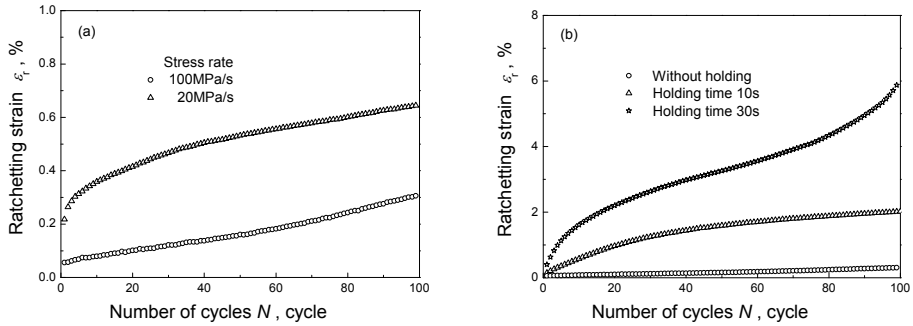

Fig. 8. Time-dependent ratchetting of the alloy at 150˚C (30±300MPa): (a) at two stress rates; (b) with or without peak stress hold. (Originally from Ding et al. (2007))

Similar to that of SS304 stainless steel observed by Kang et al. (2006), the time-dependent ratchetting of 6061-T6 aluminium alloy is also caused by the viscosity of the alloy, and the creep deformation occurred during the peak stress hold and the cyclic stressing at lower stress rate results in the increase of total ratchetting strain, which should be reasonably considered when the time-dependent ratchetting is theoretically modelled.

3.2 Ratchetting-fatigue interaction

In the former subsection, only the ratchetting behaviour of 6061-T6 aluminium alloy is discussed within relatively fewer numbers of cycles, i.e., fewer than 200 cycles. The effect of fatigue damage on the cyclic responses of the alloy has not been involved. In this subsection, the whole-life ratchetting of the alloy is investigated by the cyclic stressing tests till the fracture of the alloy occurs, in order to reveal the ratchetting-fatigue interaction of the alloy at room temperature.

At first, the whole-life ratchetting of the alloy is investigated by the tests with various stress levels (where, the mean stress is 20MPa, and the stress amplitudes are 320, 325 and 330MPa, respectively; the stress rate is 200MPa·s^{-1}). The results obtained at room temperature are shown in Fig. 9.

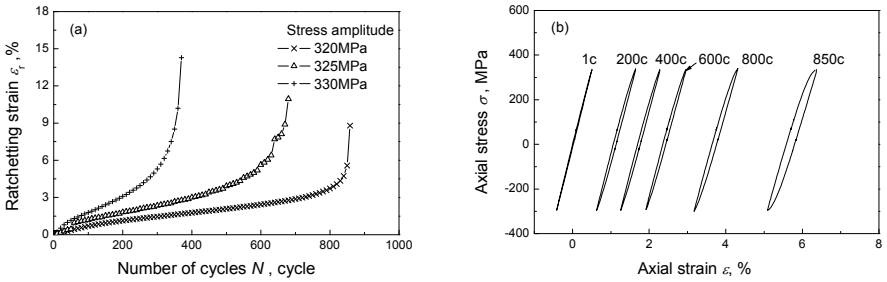

Fig. 9. Whole-life ratchetting of the alloy at room temperature: (a) curves of ratchetting strain vs number of cycles with various stress amplitudes; (b) hysteresis loops obtained in the stress cycling with 20±320MPa. (Originally from Kang et al. (2008))

It is concluded from Fig. 9 that the whole-life ratchetting evolution of 6061-T6 aluminium alloy during uniaxial cyclic stressing can be divided into three stages with respect to the variation of ratchetting strain rate, i.e., the first stage with decreasing ratchetting strain rate, second stage with an almost constant ratchetting strain rate and the third stage with quickly increasing ratchetting strain rate, as shown in Fig. 9a. Very large ratchetting strain is caused in the alloy by the stress cycling with non-zero mean stress after certain cycles, even if the initial ratchetting strain produced in the first beginning of cyclic loading is very small since the applied maximum stress is very close to the yielding strength of the alloy (i.e., about 350MPa). The re-acceleration of ratchetting deformation in the third stage of ratchetting evolution is mainly caused by the apparent fatigue damage after certain cycles and the cyclic softening feature of the alloy. It is also concluded that the increase of stress amplitude speeds up the evolution of whole-life ratchetting, the first and second stages are ended and the third stage appears more quickly, and then the material fractures within fewer cycles. It implies that the fatigue life also depends upon the applied stress amplitude, and is remarkably shortened by the increase of stress amplitude; simultaneously, the fatigue damage accelerates the evolution of ratchetting, and causes the quick occurrence of the third stage of ratchetting evolution as shown in Fig. 9a. From Fig. 9b, it is seen that the hysteresis loops gradually change from nearly linear type to apparent nonlinear ones and will become fatter and fatter during the stress cycling due to the cyclic softening feature of the alloy and the fatigue damage caused by the cyclic loading after certain number of cycles.

Secondly, the whole-life ratchetting of the alloy is observed in the tests at varied stress rate and with or without peak and/or valley stress hold, and the time-dependent ratchetting-fatigue interaction is discussed. The results at room temperature are shown in Fig. 10. Two kinds of loading charts are employed in the tests: one is composed of the tension and compression parts (simplified as T and C in Fig. 10a, respectively) at identical stress rate, which is signed as Type I; while the other is composed of the tension and compression parts at different stress rates, which is signed as Type II.

It is seen from Fig. 10a (loading case: 20±330MPa) that the evolution of whole-life ratchetting at lower stress rate is faster than that at faster stress rate in the stress cycling with the Type I loading chart, and the alloy fails within fewer cycles, even if the magnitude of final ratchetting strain at lower stress rate is lower. In the stress cycling with the Type II loading

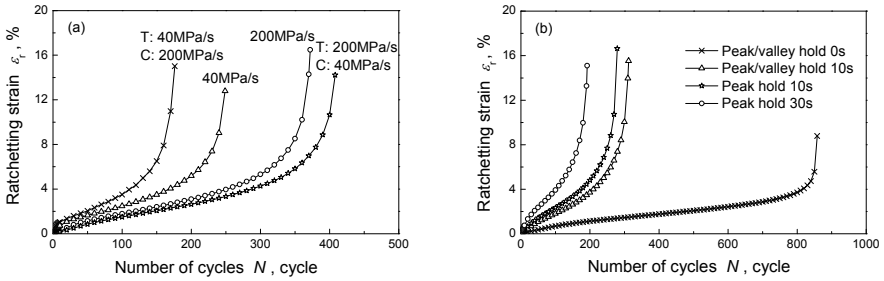

Fig. 10. Time-dependent whole-life ratchetting at room temperature: (a) at different stress rates; (b) with different hold-times at peak (/valley) stress point. (Originally from Kang et al. (2008))

chart, the evolution of ratchetting is much quicker for the case at lower stress rate in the tension part than that at quicker stress rate in the tension part, which also results in a shorter fatigue life. It is concluded that the evolution of whole-life ratchetting and fatigue life of 6061-T6 aluminium alloy depends greatly on the stress rate and its loading sequence.

The peak/valley stress hold also influences greatly the evolution of whole-life ratchetting and fatigue life of the alloy as shown in Fig. 10b. The evolution of whole-life ratchetting is accelerated and then the fatigue life is shortened by the peak or peak/valley stress hold, which becomes more remarkable when the hold time is longer. It is mainly caused by the creep strain produced during the peak stress hold. It is also shown that the fatigue life of alloy is shorter in the stress cycling with only peak stress hold than that with peak/valley stress hold. The reason is straightforward, since the stress at valley point is compressive.

To illustrate further the effect of creep deformation on the ratchetting-fatigue interaction, the alloy is tested in the stress cycling interrupted by a peak stress hold after every 50 cycles at room temperature. It is seen from Fig. 11 (loading case: 20±325MPa) that the evolution of whole-life ratchetting is accelerated and the fatigue life is shortened greatly by such stress hold, and both of them become more remarkable if the hold time is longer, even if the final ratchetting strain is almost the same for the cases with hold times of 120 and 60 seconds. It should be noted from the experimental results that the total creep strain produced at all the

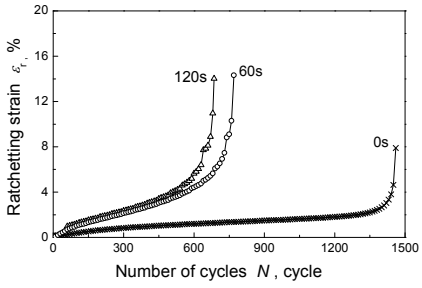

Fig. 11. Time-dependent whole-life ratchetting in interrupted stress cycling with different hold-times. (Originally from Kang et al. (2008))

interrupting peak stress holds is less than 1.0%.Therefore, the difference of final ratchetting strain between the cases with or without interrupting peak stress hold is not mainly caused by the creep strain produced during the hold. However, such small amount of creep strain causes the great increase of ratchetting strain and decrease of fatigue life. It implies that the additional creep is very detrimental to the fatigue life of the alloy in the stress cycling.

4. Time-dependent constitutive model

As commented by Kan et al. (2007), a good candidate for modelling the time-dependent ratchetting of the materials is the nonlinear kinematic hardening rule with a static recovery term. Therefore, the Kang-Kan model (Kan et al., 2007) is extended to predict the uniaxial time-dependent ratchetting of cyclic softening materials by employing a new combined nonlinear kinematic hardening rule (i.e., combination of the A-F model (Armstrong and Frederick, 1966) and Ohno-Wang model II (Ohno and Wang, 1993a)) with a static recovery term and introducing an additional nonlinear isotropic hardening rule to capture the effect of cyclic softening feature on the ratchetting (Ding et al., 2010). The developed model (Ding et al., 2010) is outlined in this chapter as follows

4.1 Main equations

In the framework of infinitesimal visco-plasticity, it is assumed that the total strain can be divided additively into elastic and inelastic strains for the isothermal case. The main equations of the proposed visco-plastic constitutive model are the same as those of the Kang-Kan model (Kan et al., 2007) and listed as follows:

$$\boldsymbol{\varepsilon} = \boldsymbol{\varepsilon}^{e} + \boldsymbol{\varepsilon}^{in} \tag{2}$$

$$\boldsymbol{\varepsilon}^{e} = \mathbf{D}^{-1} : \boldsymbol{\sigma} \tag{3}$$

$$\dot{\boldsymbol{\varepsilon}}^{in} = \sqrt{\frac{3}{2}} \left\langle \frac{F_y}{K} \right\rangle^{n} \frac{\mathbf{S} - \boldsymbol{\alpha}}{\left\| \mathbf{S} - \boldsymbol{\alpha} \right\|} \tag{4}$$

$$F_y = \sqrt{1.5(\mathbf{S} - \boldsymbol{\alpha}) : (\mathbf{S} - \boldsymbol{\alpha})} - Q \tag{5}$$

Where $\boldsymbol{\varepsilon}$, $\boldsymbol{\varepsilon}^{e}$, $\boldsymbol{\varepsilon}^{in}$ and $\dot{\boldsymbol{\varepsilon}}^{in}$ are second-ordered total strain, elastic strain, inelastic strain and inelastic strain rate tensors, respectively; $\mathbf{D}$ is the fourth-ordered elasticity tensor; K and n are temperature-dependent material parameters representing the viscosity of the material at different temperatures; $\mathbf{S}$, $\boldsymbol{\alpha}$ and Q represent deviatoric stress, back stress and isotropic deformation resistance, respectively. Hereafter, bold capital Roman alphabet represents fourth-ordered tensor, and other bold letters denote second-ordered tensors. The symbol $\langle\cdot\rangle$ denotes Macaulay bracket and means that: as $x \le 0$, $\langle x \rangle = 0$; as $x > 0$, $\langle x \rangle = x$.

4.2 Kinematic hardening rule

The non-linear kinematic hardening rule employed in the Kang-Kan model (Kan et al., 2007) is modified as a combination of the A-F model (Armstrong and Frederick, 1966) and Ohno-Wang model II (Ohno and Wang, 1993a) to describe the continuously decreasing ratchetting strain rate within certain cycles reasonably, i.e.,

$$\boldsymbol{\alpha} = \sum_{k=1}^{M} \boldsymbol{\alpha}^{(k)} \tag{6}$$

where $\boldsymbol{\alpha}$ is total back stress tensor and is divided into M components denoted as $\boldsymbol{\alpha}^{(k)}$ (k=1, 2, …, M). The evolution equation of each back stress component is expressed as:

$$\dot{\boldsymbol{\alpha}}^{(k)} = \zeta^{(k)} \left\{ \frac{2}{3} r^{(k)} \dot{\boldsymbol{\varepsilon}}^{in} - \mu^{(k)} \boldsymbol{\alpha}^{(k)} \dot{p} - \left(\frac{\bar{\alpha}^{(k)}}{r^{(k)}} \right)^{m} \left\langle \dot{\boldsymbol{\varepsilon}}^{in} : \mathbf{K}^{(k)} - \mu^{(k)} \dot{p} \right\rangle \boldsymbol{\alpha}^{(k)} \right\} - \chi^{(k)} (\bar{\alpha}^{(k)})^{\beta(k)-1} \boldsymbol{\alpha}^{(k)} \tag{7}$$

Where, $\zeta^{(k)}$ and $r^{(k)}$ are temperature-dependent material parameters; (:) indicates the inner product between second-ordered tensors; $\mathbf{K}^{(k)} = \dfrac{\boldsymbol{\alpha}^{(k)}}{\bar{\alpha}^{(k)}}$ represents the orientation of back stress component, where $\bar{\alpha}^{(k)} = (\dfrac{3}{2} \boldsymbol{\alpha}^{(k)} : \boldsymbol{\alpha}^{(k)})^{1/2}$ is the magnitude of each back stress component; $\dot{p} = (\dfrac{2}{3} \dot{\boldsymbol{\varepsilon}}^{in} : \dot{\boldsymbol{\varepsilon}}^{in})$ is the accumulated inelastic strain rate. $\mu^{(k)}$ is called as ratchetting parameter and is assumed to be identical for all the back stress components, i.e., $\mu^{(k)} = \mu$. It is also assumed that μ is a temperature-dependent material parameter and can be determined by trial-and-error method from one of the uniaxial ratchetting results. The static recovery term $-\chi^{(k)} (\bar{\alpha}^{(k)})^{\beta(k)-1} \boldsymbol{\alpha}^{(k)}$ is used to represent the static recovery effect of the alloy produced during the peak/valley stress hold. For simplicity, it is assumed that $\chi^{(k)} = \chi$ and $\beta(k) = \beta$. The parameters χ and β control the degree of static recovery occurred during the peak stress hold and are temperature-dependent.

4.3 Isotropic hardening rule

To describe the effect of cyclic softening feature on the ratchetting of the alloy, a nonlinear isotropic hardening rule is adopted in the work, i.e., for the isothermal case

$$\dot{Q} = \gamma (Q_{sa} - Q) \dot{p} \tag{8}$$

where, Q_{sa} is the saturated isotropic deformation resistance of the material presented in a specific cyclic loading and is assumed as a constant for simplicity. In Eq. (8), if $Q_{sa}<Q_0$, a decreasing isotropic deformation resistance Q is modelled, which means that the material presents a cyclic softening feature during the cyclic loading. However, if we set that $Q_{sa}>Q_0$ as done in the previous work (Kan et al., 2007), the cyclic hardening feature of SS304 stainless steel can be modelled by Eq. (8). Also, if $Q_{sa}=Q_0$, Eq. (8) represents a cyclic stable feature, which is suitable for some materials such as U71Mn rail steel (Kang, 2004). The parameter γ controls the evolution rate of isotropic deformation resistance Q. The Q_{sa} and γ are both temperature-dependent.

5. Simulations and discussion

5.1 Determination of material parameters

The material parameters used in the proposed constitutive model can be determined from the experimental results as follows: (1) The material parameters $\zeta^{(k)}$ and $r^{(k)}$ are determined

directly from the stress-plastic strain curves of monotonic tension at moderate strain rate (e.g., 0.2%·s^{-1}) by using the method described in Kang et al. (2002). (2) The material constants K and n are determined by fitting the monotonic tensile stress-strain curves at several strain rates and at room or elevated temperature. (3) Q_{sa} is determined from one of uniaxial symmetrical strain-controlled cyclic experiments with moderate strain amplitude (e.g., 0.7%) and at moderate strain rate (e.g., 0.2%·s^{-1}). (4) μ and m are obtained by trial-and-error method from one of uniaxial ratchetting results. (5) χ and β are determined from the cyclic stress-strain curves with peak/valley stress hold by trials-and-errors method at certain temperature. Besides, M=8 is used in order to simulate the ratchetting more accurately, as Kan et al (Kan et al., 2007) did. All the parameters used in the model are listed in Table 1.

Room temperature	M=8, Q_0=260MPa, K=90MPa, n=13, μ=0.01, v=0.33, E=76GPa, m=10, Q_{sa}=255MPa, γ=4; $\xi^{(1)}$=10000, $\xi^{(2)}$=2083, $\xi^{(3)}$=649, $\xi^{(4)}$=359.7, $\xi^{(5)}$=207, $\xi^{(6)}$=101, $\xi^{(7)}$=50.8, $\xi^{(8)}$=25; $r^{(1)}$=2.51, $r^{(2)}$=25.8, $r^{(3)}$=4.39, $r^{(4)}$=2.3, $r^{(5)}$=1.68, $r^{(6)}$=3.94, $r^{(7)}$=3.92, $r^{(8)}$=22.66(MPa); χ=7.9e-10MPa^{-1}, β=3.5.
150℃	M=8，Q_0=230MPa, K=80MPa, n=10, μ=0.005, v=0.33, E=75.6GPa, m=13, Q_{sa}=225MPa, γ=3; $\xi^{(1)}$=6666, $\xi^{(2)}$=2016, $\xi^{(3)}$=909, $\xi^{(4)}$=333, $\xi^{(5)}$=147, $\xi^{(6)}$=74.6, $\xi^{(7)}$=32.5, $\xi^{(8)}$=18.2; $r^{(1)}$=21.78, $r^{(2)}$= 23.84, $r^{(3)}$=17.16, $r^{(4)}$=1.11, $r^{(5)}$=5.07, $r^{(6)}$=1.93, $r^{(7)}$=12.08, $r^{(8)}$=16.38(MPa); χ=1.2e-10MPa^{-1}, β=3.

Table 1. Material parameters used in the proposed model

It should be noted that except for the parameters χ and β, other parameters used in the proposed model are determined from the experimental results obtained without any peak/valley stress/strain hold, where the effect of static recovery term can be ignored for simplicity.

5.2 Simulations and discussion

At first, it is seen from Fig. 12 that the monotonic tensile stress-strain responses of the alloy at two different strain rates are simulated by the proposed model well. However, since the static recovery term is neglected when the material parameters (except for χ and β) are determined from the monotonic tensile experiments, the simulated stress-strain responses by the proposed model with static recovery term are somewhat lower than the experimental ones in some cases.

Secondly, the cyclic stress-strain responses of the 6061-T6 aluminium alloy presented under the uniaxial strain-controlled cyclic loading with or without peak and valley strain holds are also simulated by the proposed model at two described temperatures. The results in Fig. 13 show that: (1) The cyclic softening feature is predicted reasonably by the model due to the employment of a nonlinear isotropic hardening rule describing the cyclic softening behaviour at two prescribed temperatures; (2) The effect of peak/valley strain holds on the responded stress amplitude is described reasonably by the model due to its kinematic hardening rule with a static recovery term.

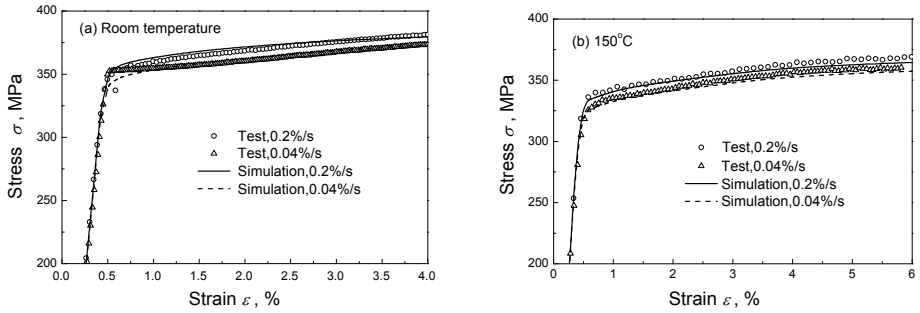

Fig. 12. Experimental and simulated results of monotonic tensile stress-strain curves of 6061-T6 aluminium alloy at two strain rates: (a) at room temperature; (b) at 150°C. (Originally from Ding et al. (2010))

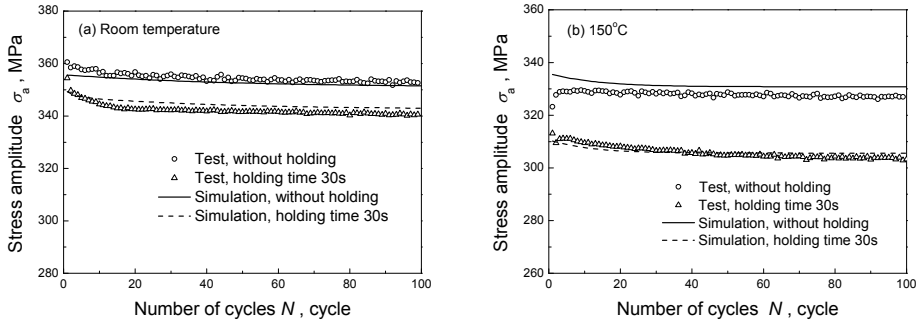

Fig. 13. Experimental and simulated results of responded stress amplitude vs. number of cycles for 6061-T6 aluminium alloy in the uniaxial symmetrical strain-controlled cyclic loading with strain amplitude of 0.6% and varied hold-time at peak and valley strains: (a) at room temperature; (b) at 150°C. (Originally from Ding et al. (2010))

Finally, the time-dependent ratchetting of 6061-T6 aluminium alloy is simulated by the proposed model, and the simulated results for different loading cases are shown in Fig. 14 to Fig. 17.

It is concluded from the figures that: (1) The effects of applied mean stress and stress amplitude on the uniaxial ratchetting of the alloy are reasonably described by the proposed model at room temperature and 150°C, as shown in Fig. 14 and Fig. 15. (2) The time-dependent ratchetting behaviours of the alloy presented at different stress rates and with or without peak stress holds are well predicted by the proposed model as shown in Fig. 16 and Fig. 17, due to the addition of the static recovery term into the nonlinear kinematic hardening rule.

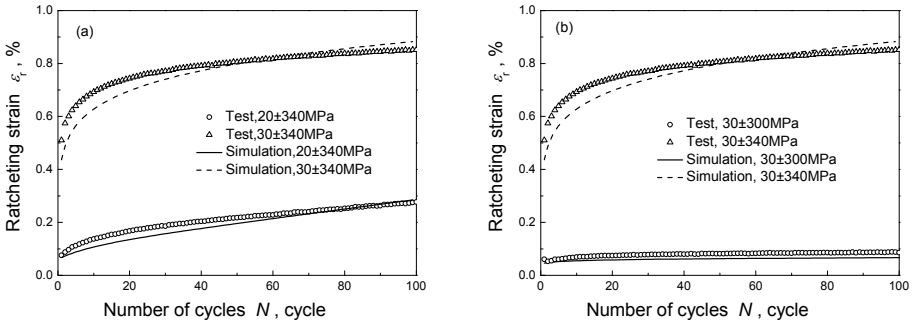

Fig. 14. Experimental and simulated results of uniaxial ratcheting for 6061-T6 aluminium alloy at room temperature (stress rate 100MPa·s^{-1}): (a) with different mean stresses; (b) with different stress amplitudes. (Originally from Ding et al. (2010))

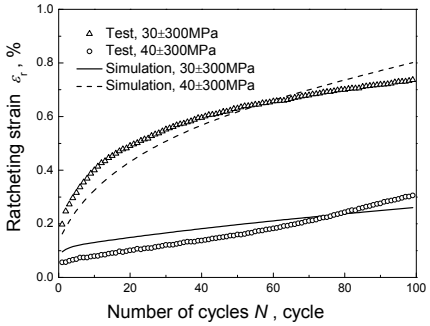

Fig. 15. Experimental and simulated results of uniaxial ratcheting for 6061-T6 aluminium alloy at 150˚C and with different mean stresses (stress rate 100MPa·s^{-1}). (Originally from Ding et al. (2010))

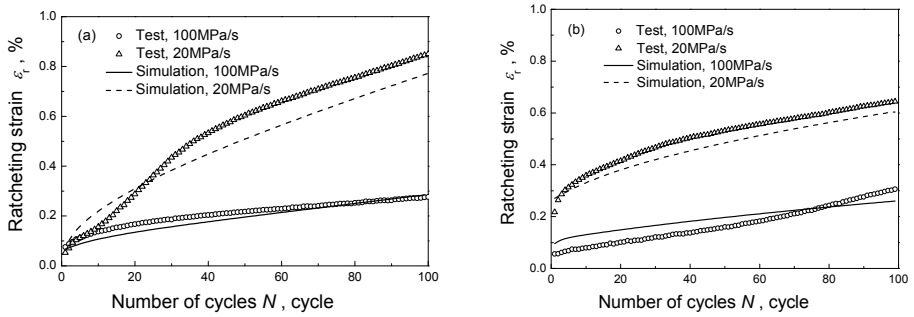

Fig. 16. Experimental and simulated results of time-dependent ratchetting for 6061-T6 aluminium alloy at two stress rates: (a) 20±340MPa, at room temperature; (b) 30±300MPa, at 150˚C. (Originally from Ding et al. (2010))

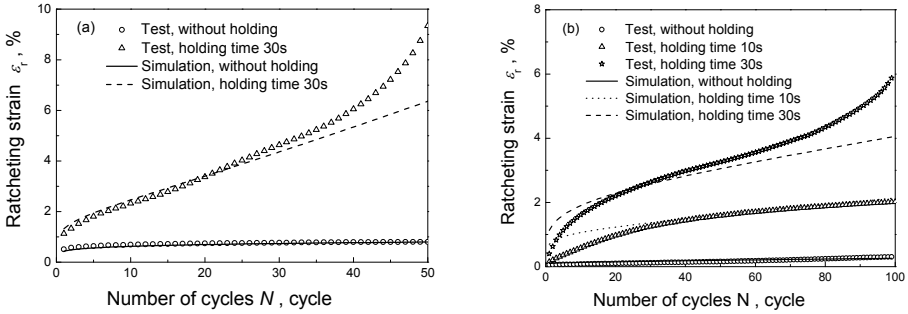

Fig. 17. Experimental and simulated results of time-dependent ratchetting of 6061-T6 aluminium alloy with different hold-times at peak stress (stress rate 100MPa·s^{-1}): (a) 30±340MPa, at room temperature; (b) 30±300MPa, at 150°C. (Originally from Ding et al. (2010))

From the simulated results shown in Fig. 14 to Fig. 17, it can be obtained that the decreasing ratchetting strain rate with the increasing number of cycles observed in the experimental results of 6061-T6 aluminium alloy within certain cycles is simulated reasonably by the proposed model employing the nonlinear kinematic hardening rule combining A-F model and Ohno-Wang model II. The decreasing rate of ratchetting strain is reasonably described by the power function $\left(\frac{\overline{\alpha}^{(k)}}{r^{(k)}}\right)^m$ used in the proposed model, while the Heaviside function $H(f^{(k)})$ used in the Kang-Kan model (Kan et al. 2007) just can provide a constant rate of ratchetting strain.

It should be noted that in the cases with peak stress hold for 30s at room temperature and 150°C, the experimental phenomenon that the ratchetting strain rate re-increases quickly with the increasing number of cycles after certain cycles as shown in Fig. 17a and 17b cannot be precisely predicted by the proposed model. As mentioned in Section 3, the re-acceleration of ratchetting deformation in these cases is mainly caused by the interaction of cyclic softening feature and fatigue damage after certain cycles. However, the proposed model neglects the evolution of fatigue damage and its effect on the ratchetting of the alloy. Therefore, although the cyclic softening feature of the alloy has been reasonably considered in the proposed model as shown in Fig. 13, the model cannot provide a precise simulation to the re-acceleration of ratchetting strain rate as shown in Fig. 17. The constitutive model

considering the interaction of ratchetting and fatigue damage will be discussed in the future work for 6061-T6 aluminium alloy in the framework of finite deformation, because the final ratchetting strains in some cases are much larger than 10% as shown in Figs. 9 to 11. Furthermore, only the uniaxial time-dependent ratchetting of 6061-T6 aluminium alloy is discussed in this work with the assumption of isothermal deformation. The multiaxial time-dependent ratchetting and that in the non-isothermal case have not been considered yet. It is concluded in Kang et al. (2006) that the multiaxial time-dependent ratchetting is affected by the obvious non-proportionally additional hardening under multiaxial cyclic loading. So the non-proportionality should be considered in the model describing the multiaxial time-dependent ratchetting, which is now in progress and will be discussed in future work.

6. Conclusions and future research

Based on the works done by Ding et al. (2007), Kang et al. (2008) and Ding et al. (2010), the following conclusions are summarized for the cyclic deformation of 6061-T6 aluminium alloy at room and high temperatures: (1) The 6061-T6 aluminium alloy presents apparent cyclic softening feature, and the cyclic softening feature is time-dependent at room and high temperatures, i.e., the responded stress amplitude decreases with the increasing holding time during the cyclic straining with peak/valley strain hold. (2) Ratchetting occurs in the alloy remarkably during the cyclic stressing with non-zero mean stress. The ratchetting greatly depends on the current stress level and its loading history. The ratchetting strain increases with the increasing of applied mean stress or stress amplitude, and the previous cyclic stressing with higher stress level restrains the occurrence of ratchetting in the sequent cyclic stressing with lower stress level. (3) The ratchetting of the alloy presents remarkable time-dependence at room and high temperatures. The ratchetting strain produced during the cyclic stressing at lower stress rate or with certain peak stress hold is much higher that that at higher stress rate and without peak stress hold. The time-dependent ratchetting of the alloy is mainly caused by the creep deformation produced during the peak stress hold or at lower stress rate due to its viscosity at room and high temperatures. (4) The whole-life ratchetting evolution of the alloy at room temperature can be divided into three stages, i.e., the first stage with decreasing ratchetting strain rate, second stage with an almost constant rate and the third stage with quickly increasing rate. As a result, the fatigue life is shortened by the quicker ratchetting evolution. The creep strain produced during the peak/valley stress hold and at lower stress rate accelerates the evolution of ratchetting and shortens the low-cycle fatigue life of the alloy. (5) Based on the experimental results of time-dependent ratchetting for 6061-T6 aluminium alloy at room temperature and 150°C, a new unified visco-plastic constitutive model is proposed to predict the uniaxial time-dependent ratchetting by extending the Kang-Kan model (Kan et al., 2007). The extended kinematic hardening rule is based on the combination of the A-F model and Ohno-Wang model II, rather than that of the A-F model and Ohno-Wang model I in Kan et al. (2007), to obtain a continuously decreasing ratchetting strain rate. Comparing with the experimental results shows that the proposed model provides a good simulation to the time-dependent cyclic deformation behaviour of 6061-T6 aluminium alloy at room temperature and 150°C, including the uniaxial time-dependent ratchetting.

As a preliminary study on the ratchetting of aluminium alloys, as summarized in this chapter, the authors only perform an experimental observation on the uniaxial ratchetting and ratchetting-fatigue interaction of 6061-T6 aluminium alloy and their time-dependence, and construct a new unified visco-plastic cyclic constitutive model to describe the uniaxial time-dependent ratchetting of the alloy. Much more effort is needed to investigate the ratchetting and ratchetting-fatigue interaction of aluminium alloys in the future, especially on the topics listed as follows: (1) Experimental observation of multiaxial ratchetting and ratchetting-fatigue interaction of aluminium alloys at room and high temperatures; (2) Constitutive model of multiaxial time-dependent ratchetting; (3) Damage-coupled constitutive model and fatigue failure model of ratchetting-fatigue interaction; (4) finite element implementation of newly developed cyclic constitutive model and numerical simulation to the cyclic deformation of structure components made from aluminium alloys; (5) Micro-mechanism of ratchetting behaviour of aluminium alloys and micro-mechanism-based constitutive model.

7. Acknowledgement

The work was financially supported by National Natural Science Foundation of China (No. 10772153) and the project of "973" with contract number of 2007CB714704. AvH Foundation and Prof. O.T. Bruhns are also appreciated for their support to G.Z. Kang's staying in Germany (2009-2010) as an AvH Experienced Research Fellow.

8. References

Abdel-Karim, M. & Ohno, N. (2000). Kinematic hardening model suitable for ratchetting with steady-state, *International Journal of Plasticity*, Vol. 16, No. 2, 225-240.

Armstrong, P. & Frederick, C. (1966). A mathematical representation of multiaxial Bauschinger effect, *CEGB report rd/b/n731*, Berkely Nuclear Laboratories, Berkely, UK.

Bari, S. & Hassan, T. (2002). An advancement in cyclic plasticity modeling for multiaxial ratchetting simulation, *International Journal of Plasticity*, Vol. 18, No. 5, 873-894.

Chaboche, J. (1991). On some modifications of kinematic hardening to improve the description of ratchetting effects, *International Journal of Plasticity*, Vol. 7, No. 7, 661-678.

Chaboche, J. (2008). A review of some plasticity and viscoplasticity constitutive theories, *International Journal of Plasticity*, Vol. 24, No. 9, 1642-1693.

Chen, X. & Abel, A. (1996). A two-surface model describing ratchetting behaviours and transient hardening under nonproportional loading, *Acta Mechanica Sinica*, Vol. 12, No. 4, 368-376.

Chen, X. & Jiao, R. (2004). Modified kinematic hardening rule for multiaxial ratchetting prediction, *International Journal of Plasticity*, Vol. 20, No. 5, 871-898.

Ding, J., Kang, G., Liu, Y. & Wang, H. (2007). Uniaxial time-dependent cyclic deformation of 6061-T6 aluminium alloy, *The Chinese Journal of Nonferrous Metals*, Vol. 17, No. 12, 1993-1998. (in Chinese)

Ding, J., Kang, G., Liu, Y. & Wang, H. (2008). Study on the uniaxial cyclic deformation of LY12CZ aluminium alloy and its time-dependence, *Acta Aeronautica et Astronautica Sinica*, Vol. 29, No. 1, 70-74. (in Chinese)

Ding, J., Kang, G., Kan, Q. & Liu, Y. (2010). Constitutive model for time-dependent ratcheting behavior of 6061-T6 aluminium alloy, *Computational Materials Science*, 2010, to be submitted.

Hu, W., Wang, C. & Barter, S. (1999). Analysis of cyclic mean stress relaxation and strain ratchetting behaviour of aluminium 7050, *DSTO-RR-0153*, Aeronautical and Maritime Research Laboratory, Victoria, Australia.

Jiang, Y. & Sehitoglu, H. (1996). Modeling of cyclic ratchetting plasticity, *ASME Journal of Applied Mechanics*, Vol. 63, No. 3, 720-733.

Kan, Q., Kang, G. & Zhang, J. (2007). Uniaxial time-dependent ratchetting: visco-plastic model and finite element application, *Theoretical and Applied Fracture Mechanics*, Vol. 47, No. 2, 133-144.

Kang, G. (2004). A visco-plastic constitutive model for ratchetting of cyclically stable materials and its finite element implementation, *Mechanics of Materials*, Vol. 36, No. 4, 299-312.

Kang, G. (2008). Ratchetting: Recent progresses in phenomenon observation, constitutive modelling and application, *International Journal of Fatigue*, Vol. 30, No. 10, 1448-1472.

Kang, G., Gao, Q. & Yang X. (2002). A visco-plastic constitutive model incorporated with cyclic hardening for uniaxial/multiaxial ratchetting of SS304 stainless steel at room temperature, *Mechanics of Materials*, Vol. 34, No. 9, 521-531.

Kang, G., Kan, Q., Zhang, J. & Sun, Y. (2006). Time-dependent ratchetting experiments of SS304 stainless steel, *International Journal of Plasticity*, Vol. 22, No. 5, 858-894.

Kang, G., Liu, Y. & Ding, J. (2008). Experimental study on time-dependent ratcheting-fatigue interaction of T6-6061Al alloy, *Proceedings of FM2008*, pp. 287-291, Hangzhou, October, 2008, East China University of Science and Technology Press, Shanghai, China.

Kang, G., Liu, Y., Ding, J. & Gao, Q. (2009). Uniaxial ratcheting and fatigue failure of tempered 42CrMo steel: Damage evolution and damage-coupled visco-plastic constitutive model, *International Journal of Plasticity*, Vol. 25, No. 5, 838-860.

Kang, G., Ohno N. & Nebu, A. (2003). Constitutive modeling of strain-range-dependent cyclic hardening, *International Journal of Plasticity*, Vol. 19, No. 10, 1801-1819.

Ohno, N. (1990). Recent topics in constitutive modeling of cyclic plasticity and visco-plasticity, *Applied Mechanics Review*, Vol. 43, No. 11, 283-295.

Ohno, N. (1997). Recent progress in constitutive modelling for ratchetting, *Material Science Research International*, Vol. 3, No. 1, 1-10.

Ohno, N. & Wang, J. (1993a). Kinematic hardening rules with critical state of dynamic recovery: I. Formulation and basic features for ratchetting behavior, *International Journal of Plasticity*, Vol. 9, No. 3, 375-389.

Ohno, N. & Wang, J. (1993b). Kinematic hardening rules with critical state of dynamic recovery: II. Application to experiments of ratchetting behavior, *International Journal of Plasticity*, Vol. 9, No. 3, 390-403.

Yang, X., Gao, Q., Cai, L. & Xiang, Y. (1998). An experimental study on the ratchetting behaviour of pure aluminium under uniaxial cyclic stressing, *Acta Mechanica Solida Sinica*, Vol. 19, No. 2, 134-137.

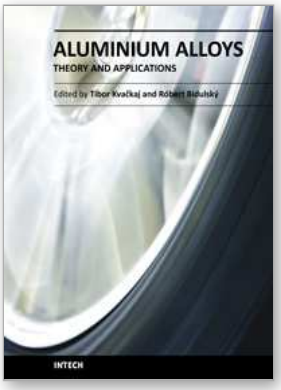

Aluminium Alloys, Theory and Applications

Edited by Prof. Tibor Kvackaj

ISBN 978-953-307-244-9
Hard cover, 400 pages
Publisher InTech
Published online 04, February, 2011
Published in print edition February, 2011

The present book enhances in detail the scope and objective of various developmental activities of the aluminium alloys. A lot of research on aluminium alloys has been performed. Currently, the research efforts are connected to the relatively new methods and processes. We hope that people new to the aluminium alloys investigation will find this book to be of assistance for the industry and university fields enabling them to keep up-to-date with the latest developments in aluminium alloys research.

InTech Europe
University Campus STeP Ri
Slavka Krautzeka 83/A
51000 Rijeka, Croatia
Phone: +385 (51) 770 447
Fax: +385 (51) 686 166
www.intechopen.com

InTech China
Unit 405, Office Block, Hotel Equatorial Shanghai
No.65, Yan An Road (West), Shanghai, 200040, China
中国上海市延安西路65号上海国际贵都大饭店办公楼405单元
Phone: +86-21-62489820
Fax: +86-21-62489821